Supporting Information

Visual Luminescence Thermometry Enabled by Phase-Transition-Activated Cross Relaxation of Tb^{3+} Ions

L. Marciniak[1*], M. Szymczak[1*]

[1] Institute of Low Temperature and Structure Research, Polish Academy of Sciences,

Okólna 2, 50-422 Wrocław, Poland

* corresponding author: l.marciniak@intibs.pl; m.szymczak@intibs.pl

KEYWORDS ratiometric thermometry, phase transition, thermal imaging, visual thermometry

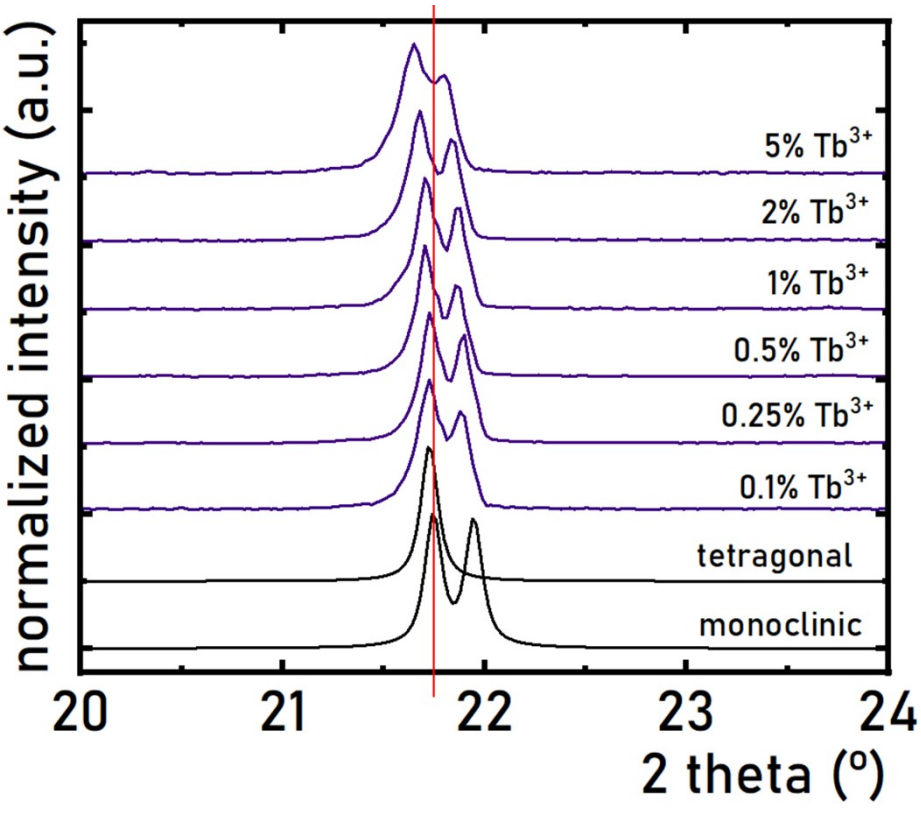

Figure S1. The zoom of the room temperature XRD spectra for $LiYO_2$:Tb^{3+} with different concentration of Tb^{3+} ions.

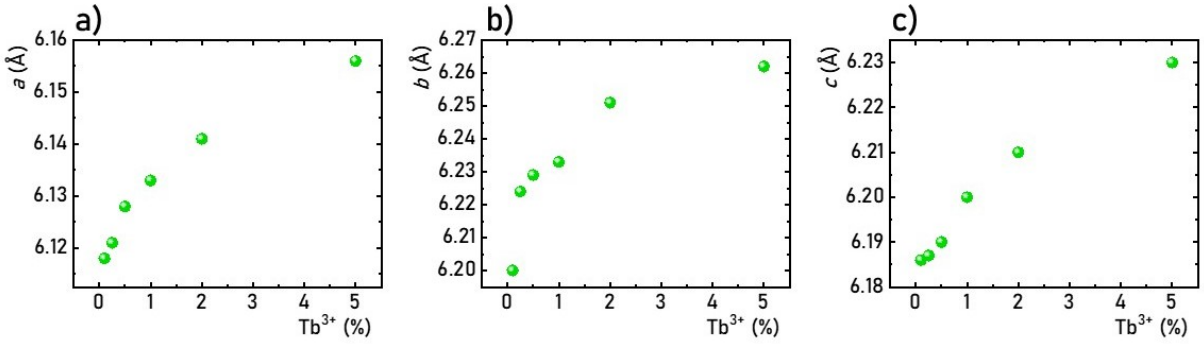

Figure S2. The influence of the Tb^{3+} ions concentration on the unit cell parameters of $LiYO_2:Tb^{3+}$ determined from Rietveld refinement of the room temperature XRD patterns.

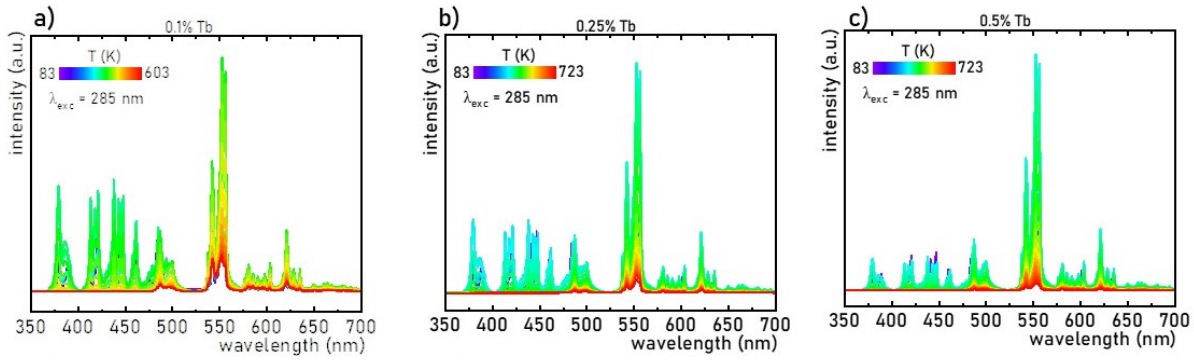

Figure S3. Thermal dependence of emission spectra of $LiYO_2:Tb^{3+}$ doped with 0.1%Tb^{3+} - a); 0.25%Tb^{3+} - b) and 0.5%Tb^{3+} - c).

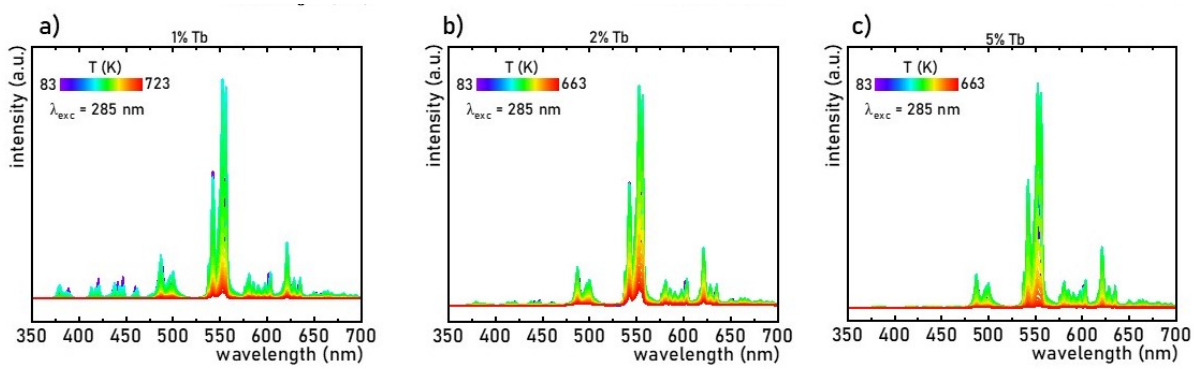

Figure S4. Thermal dependence of emission spectra of $LiYO_2:Tb^{3+}$ doped with 1%Tb^{3+} - a); 2%Tb^{3+} - b) and 5%Tb^{3+} - c).

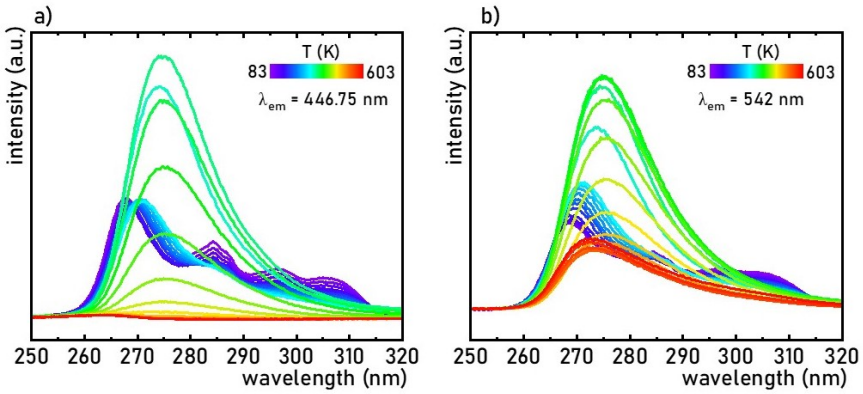

Figure S5. Thermal dependence of excitation spectra of $LiYO_2$:0.1%Tb^{3+} measured for the emission from the $^5D_3$ – a) and $^5D_4$ – b) states.

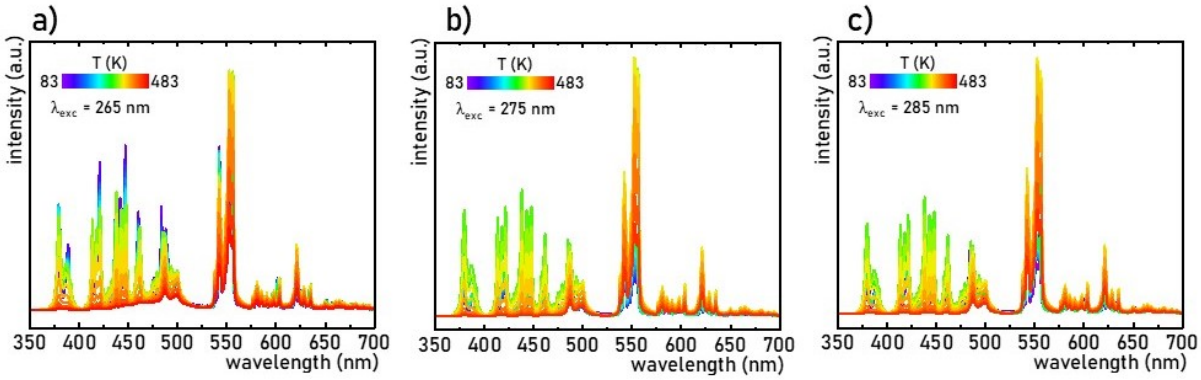

Figure S6. Thermal dependence of emission spectra of $LiYO_2$:0.1%Tb^{3+} measured under λ_{exc}=265 nm - a); under λ_{exc}=275 nm - b) and under λ_{exc}=285 nm - c).

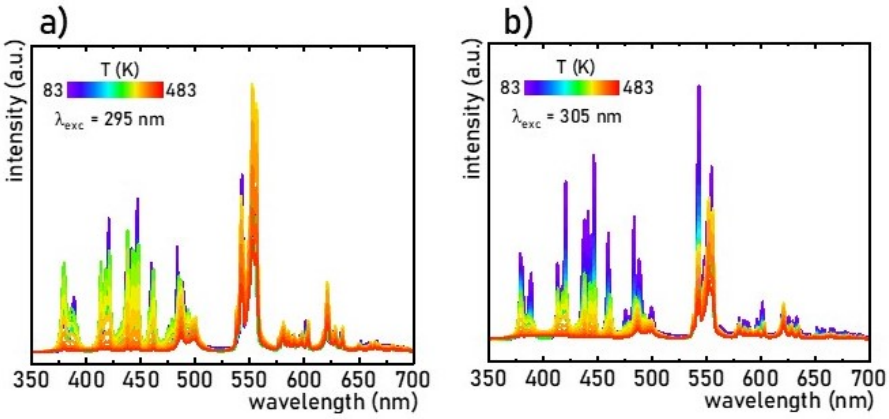

Figure S7. Thermal dependence of emission spectra of $LiYO_2$:0.1%Tb^{3+} measured under λ_{exc}=295 nm - a); under λ_{exc}=305 nm - b).

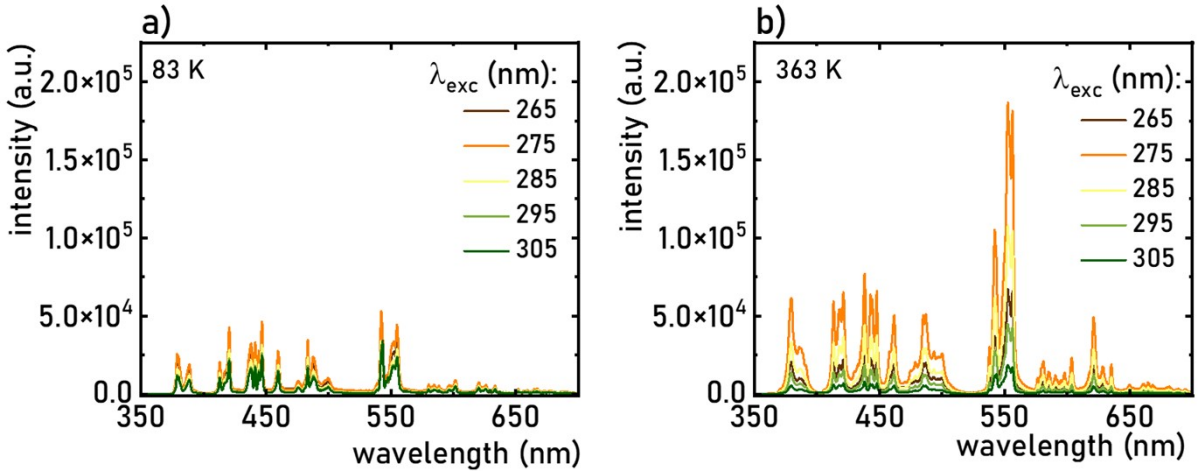

Figure S8. The comparison of the emission spectra of $LiYO_2$:0.1%Tb^{3+} measured upon different excitation wavelengths at 83K- a) and 363K – b).

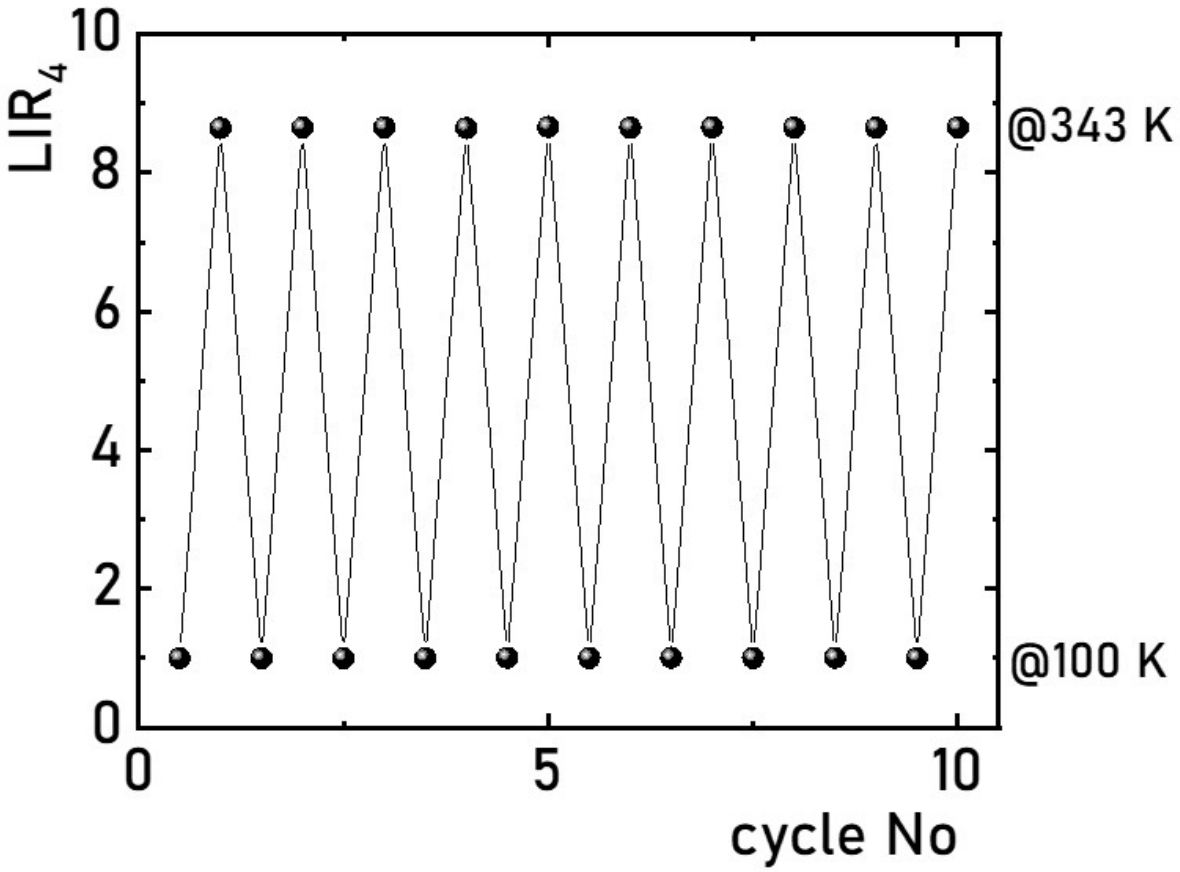

Figure S9. The LIR_4 for $LiYO_2$:0.1%Tb^{3+} within heating cooling cycles between 100 K and 343 K.

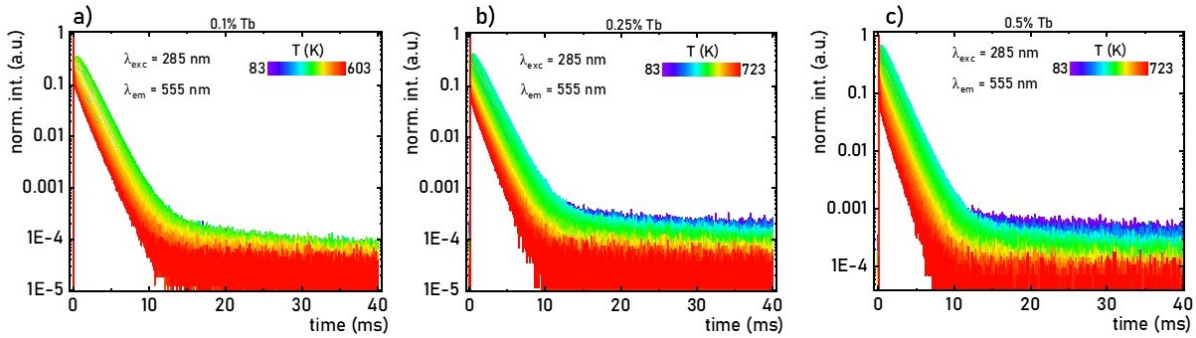

Figure S10. Thermal dependence of luminescence decay profiles measured for the emission from $^5D_4$ state of $LiYO_2$:Tb^{3+} doped with 0.1%Tb^{3+} - a); 0.25%Tb^{3+} - b) and 0.5%Tb^{3+} - c).

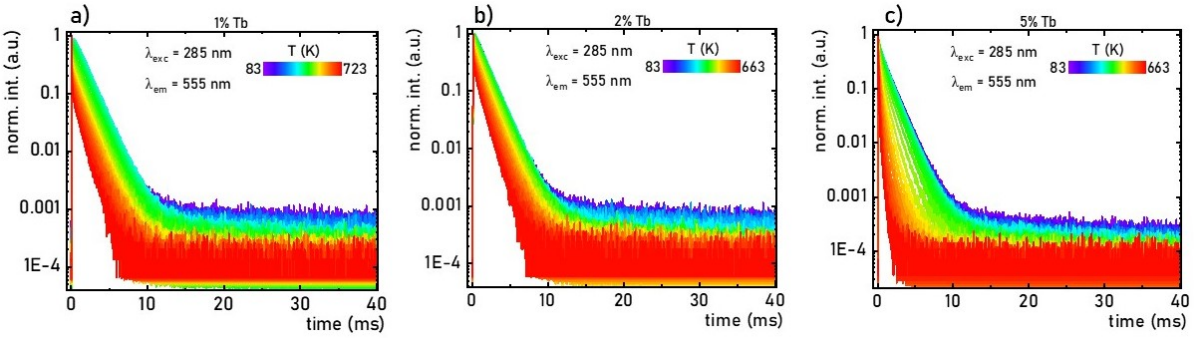

Figure S11. Thermal dependence of luminescence decay profiles measured for the emission from $^5D_4$ state of $LiYO_2$:Tb^{3+} doped with 1%Tb^{3+} - a); 2%Tb^{3+} - b) and 5%Tb^{3+} - c).

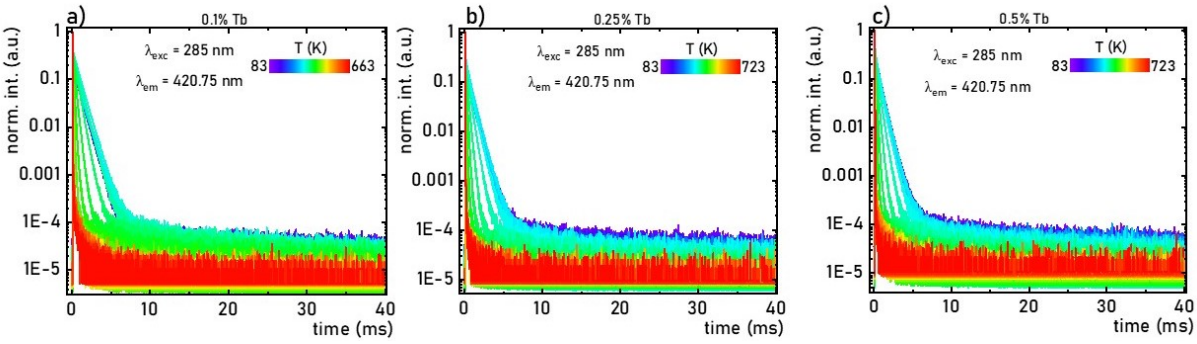

Figure S12. Thermal dependence of luminescence decay profiles measured for the emission from $^5D_3$ state of $LiYO_2$:Tb^{3+} doped with 0.1%Tb^{3+} - a); 0.25%Tb^{3+} - b) and 0.5%Tb^{3+} - c).

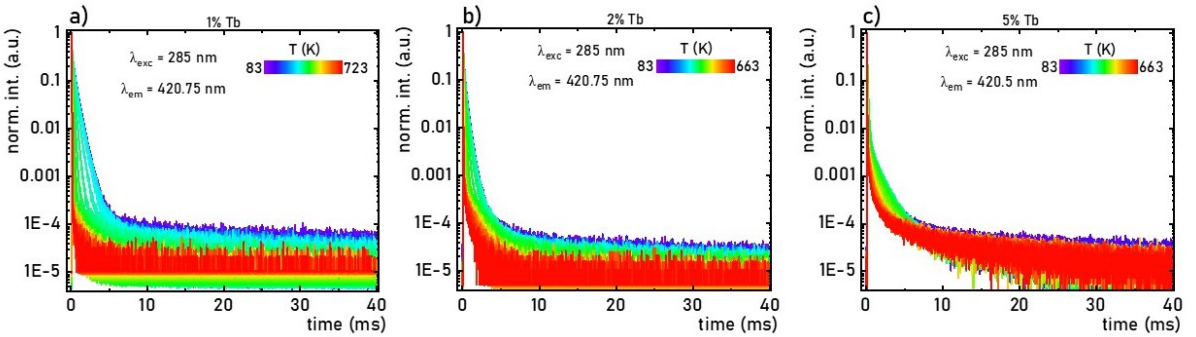

Figure S13. Thermal dependence of luminescence decay profiles measured for the emission from $^5D_3$ state of $LiYO_2:Tb^{3+}$ doped with 1%Tb^{3+} - a); 2%Tb^{3+} - b) and 5%Tb^{3+} - c).

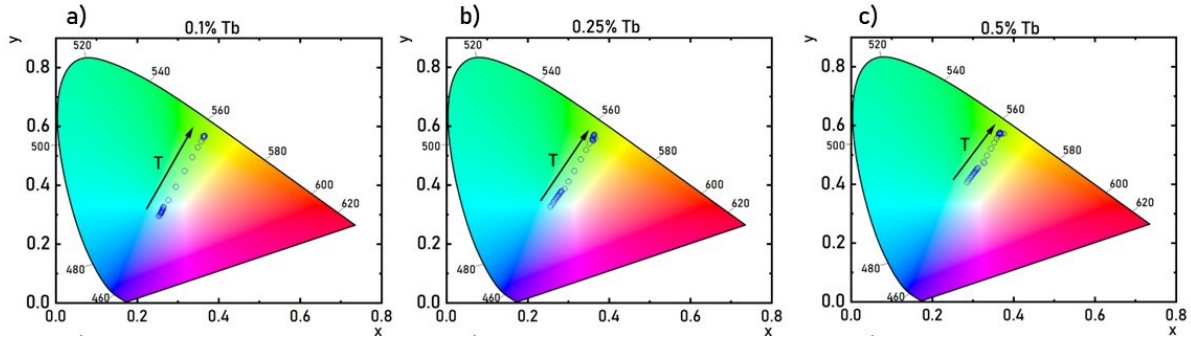

Figure S14. Thermal dependence of CIE1931 of $LiYO_2:Tb^{3+}$ doped with 0.1%Tb^{3+} - a); 0.25%Tb^{3+} - b) and 0.5%Tb^{3+} - c).

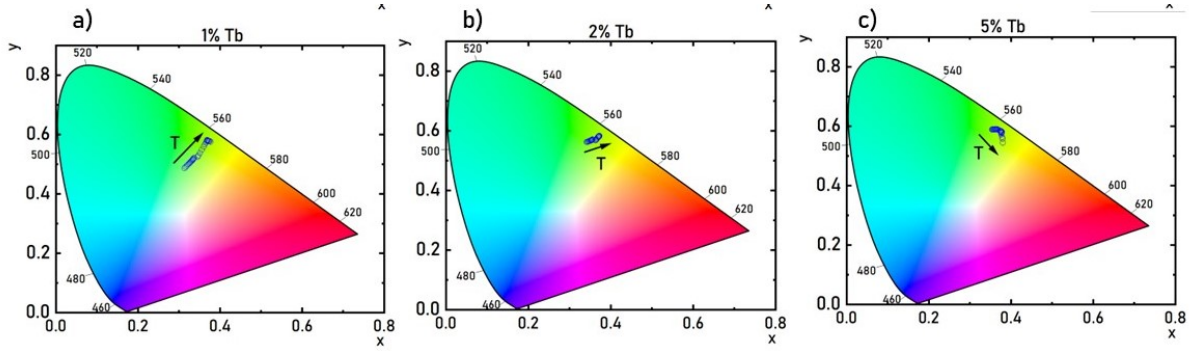

Figure S15. Thermal dependence of CIE1931 of $LiYO_2:Tb^{3+}$ doped with 1%Tb^{3+} - a); 2%Tb^{3+} - b) and 5%Tb^{3+} - c).

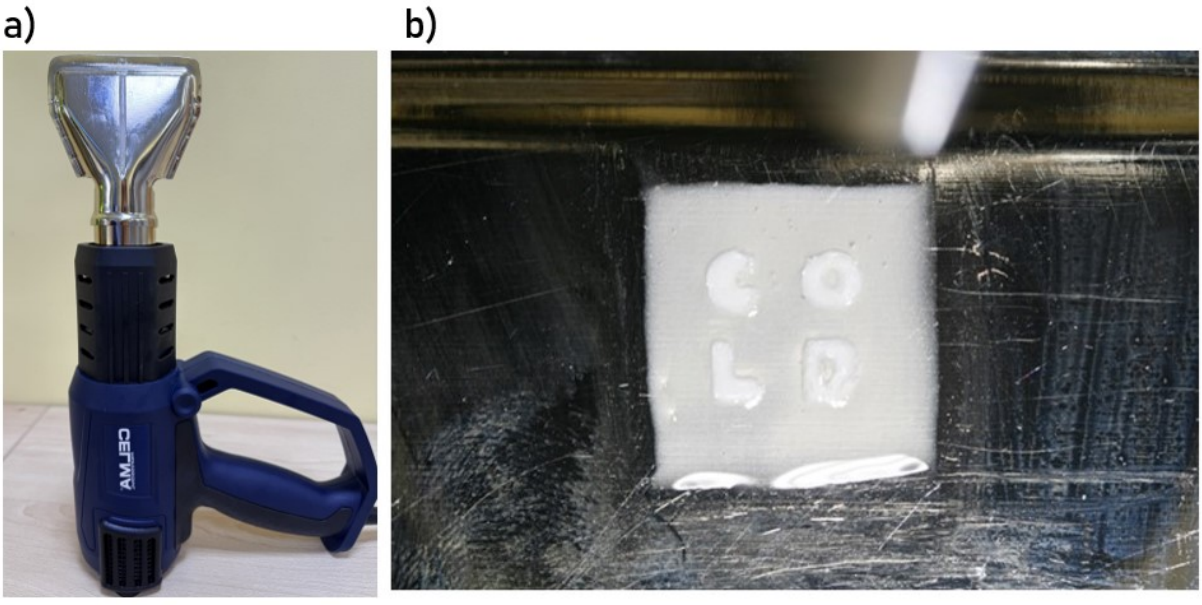

Figure S16. The bright field photo of the heat gun used in the proof of concept experiment – a) and the pattern made of the $LiYO_2$:0.1%Tb^{3+} (letters COLD) and $LiYO_2$:2%Tb^{3+} (background) – b).

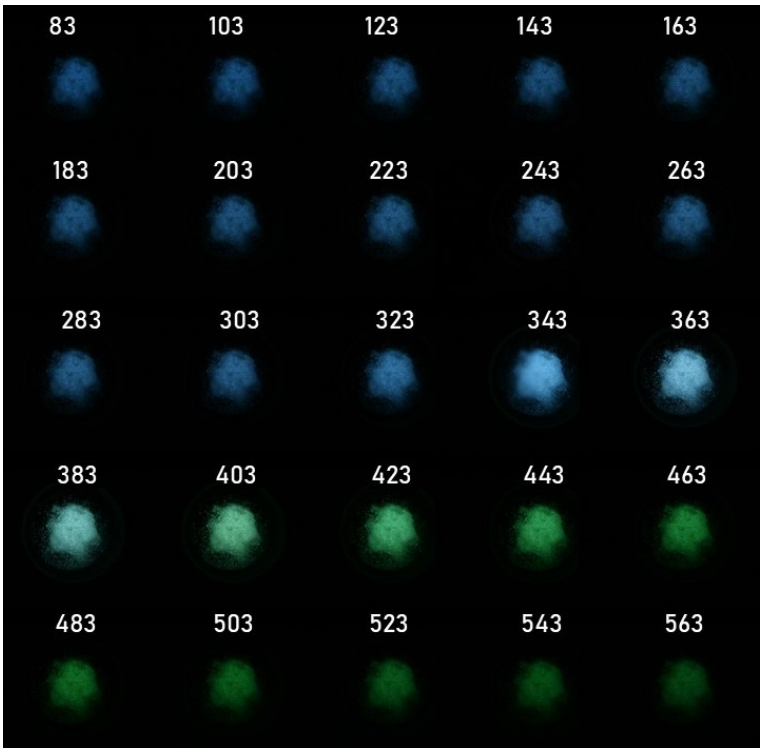

Figure S17. Photos of luminescence from $LiYO_2$:0.1%Tb^{3+} obtained under λ_{exc}=285 nm at different temperatures.

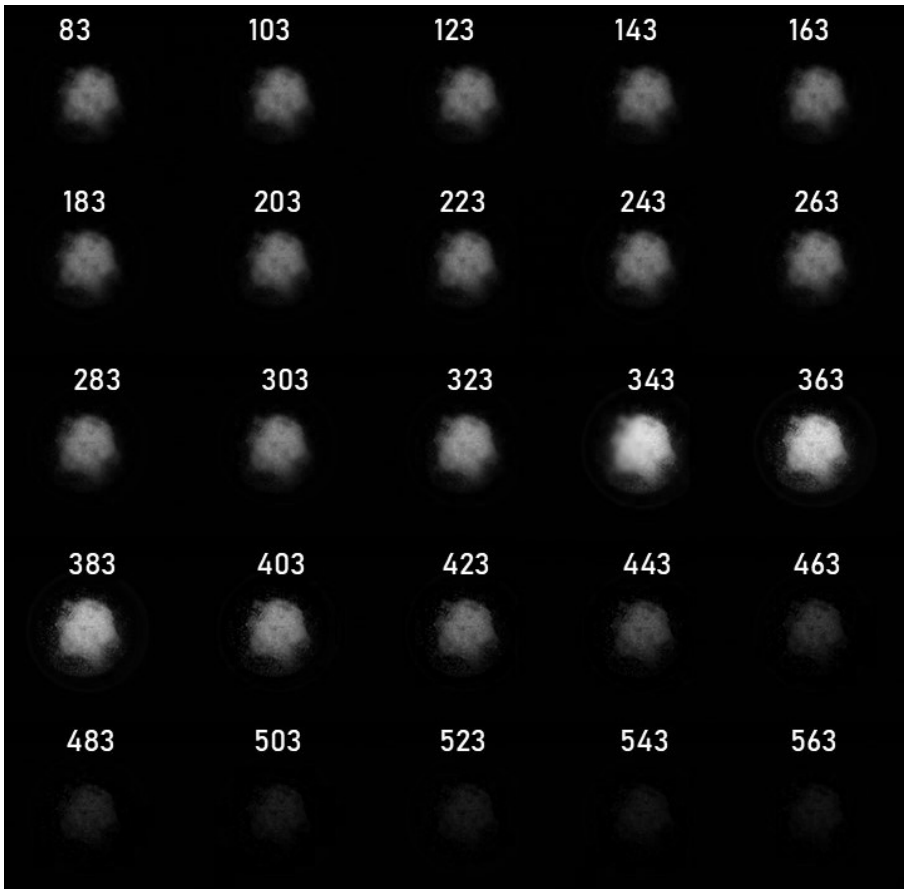

Figure S18. Intensity recorded in B channel from photos of luminescence from $LiYO_2$:0.1%Tb^{3+} obtained under λ_{exc}=285 nm at different temperatures.

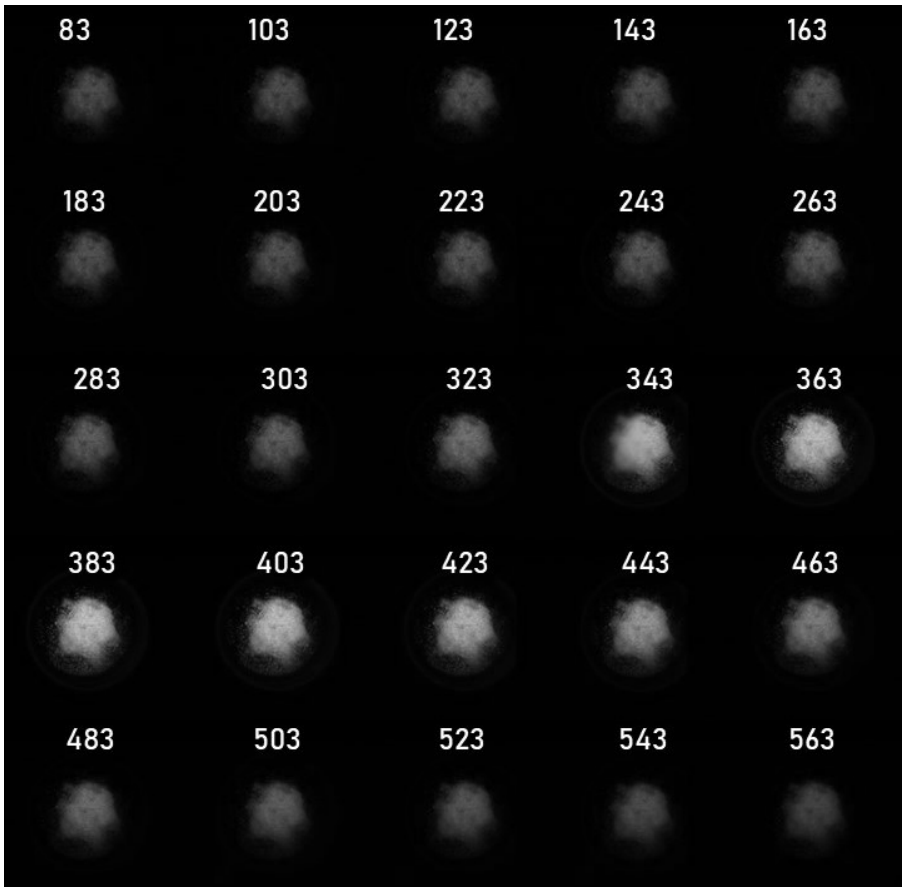

Figure S19. Intensity recorded in G channel from photos of luminescence from $LiYO_2$:0.1%Tb^{3+} obtained under λ_{exc}=285 nm at different temperatures.

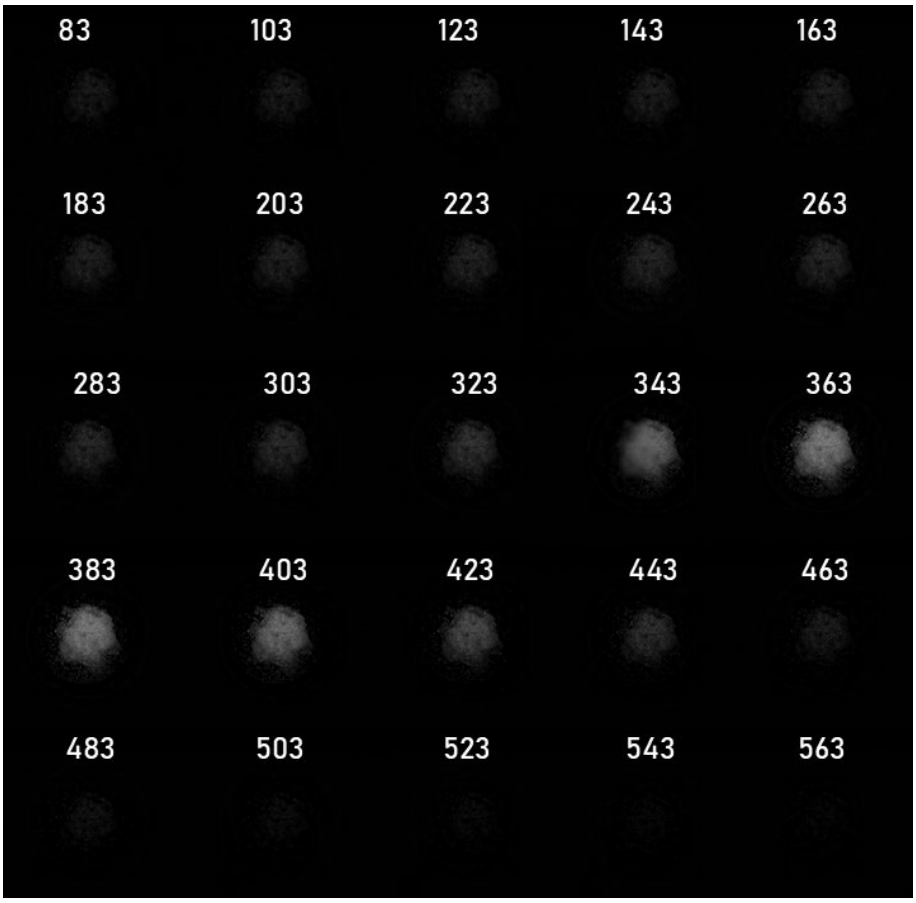

Figure S20. Intensity recorded in R channel from photos of luminescence from $LiYO_2$:0.1%Tb^{3+} obtained under λ_{exc}=285 nm at different temperatures.

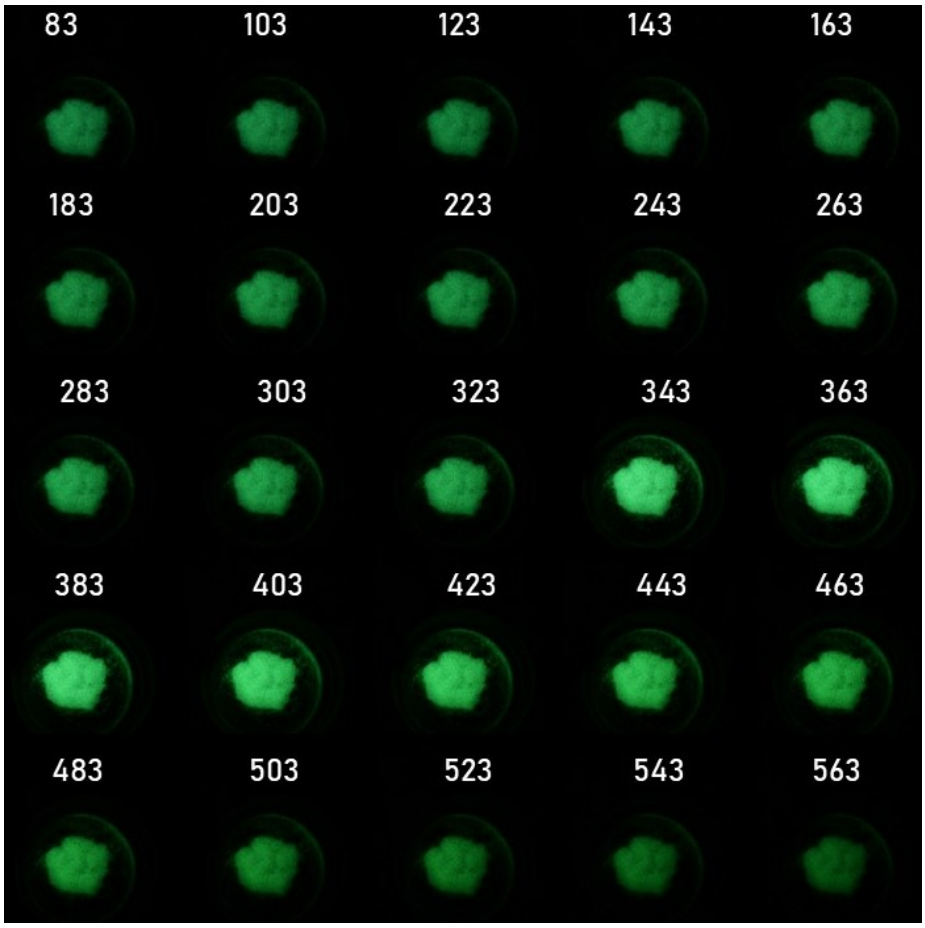

Figure S21. Photos of luminescence from $LiYO_2$:2%Tb^{3+} obtained under λ_{exc}=285 nm at different temperatures.

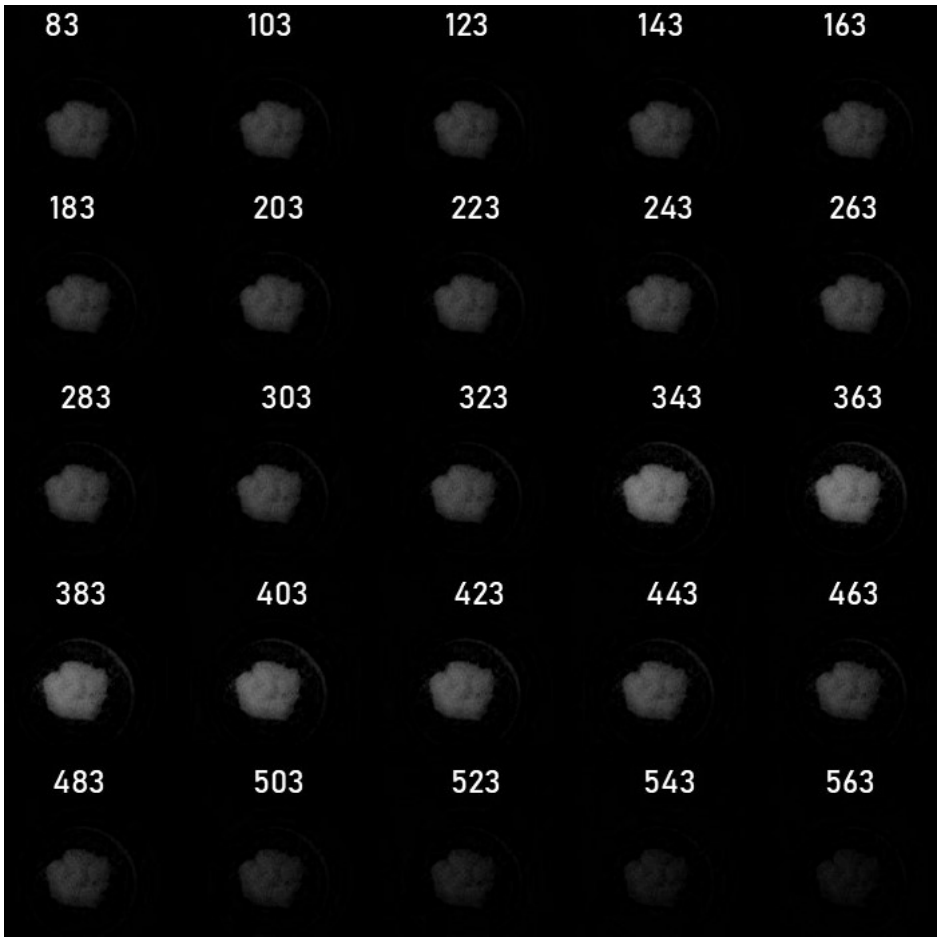

Figure S22. Intensity recorded in B channel from photos of luminescence from $LiYO_2$:2%Tb^{3+} obtained under λ_{exc}=285 nm at different temperatures.

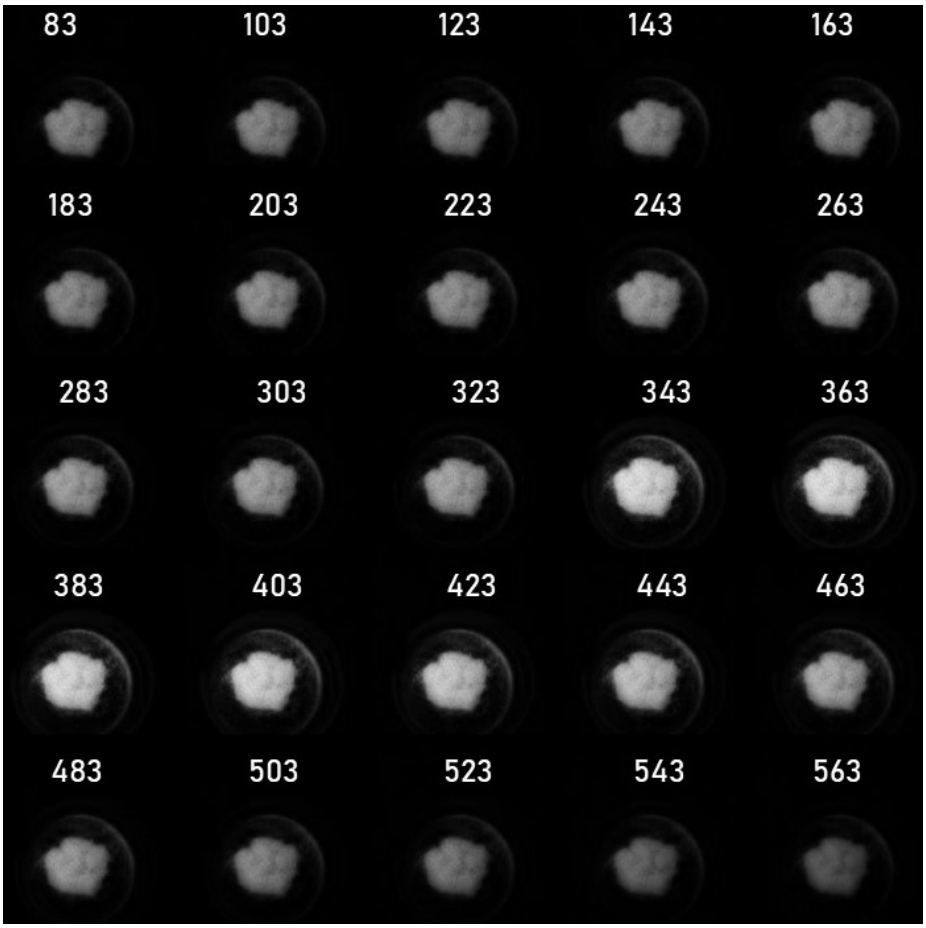

Figure S23. Intensity recorded in G channel from photos of luminescence from $LiYO_2$:2%Tb^{3+} obtained under λ_{exc}=285 nm at different temperatures.

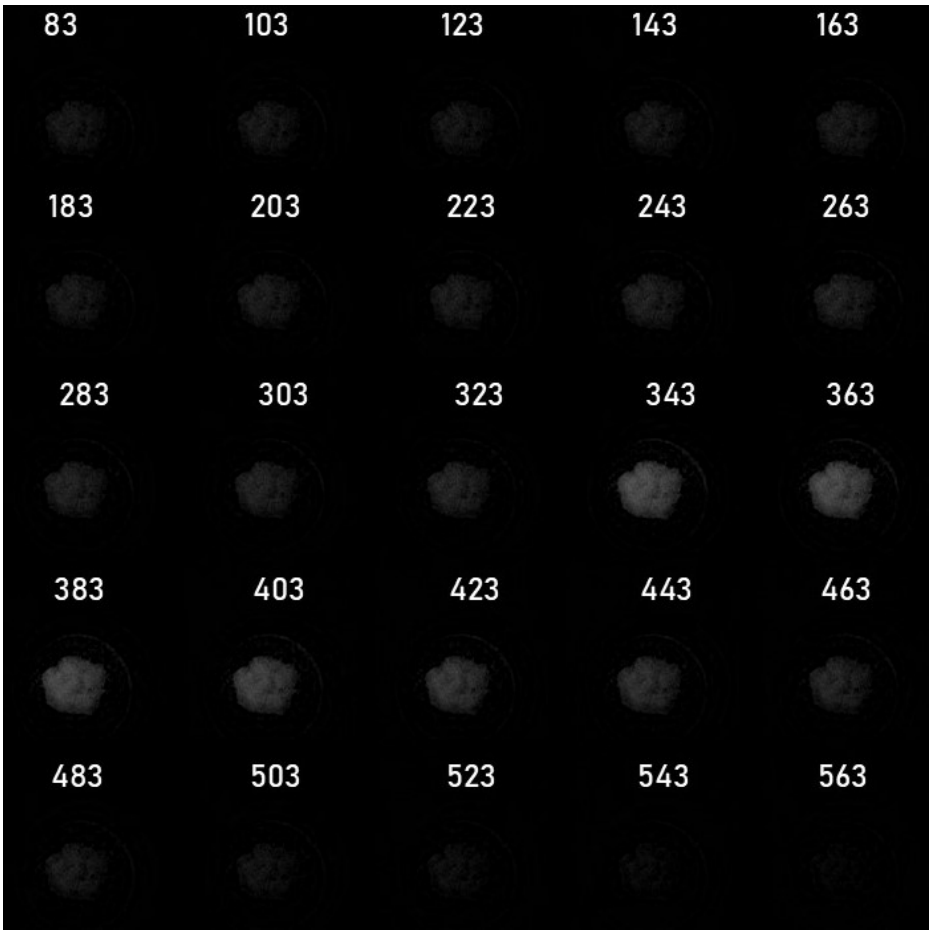

Figure S24. Intensity recorded in R channel from photos of luminescence from $LiYO_2$:2%Tb^{3+} obtained under λ_{exc}=285 nm at different temperatures.

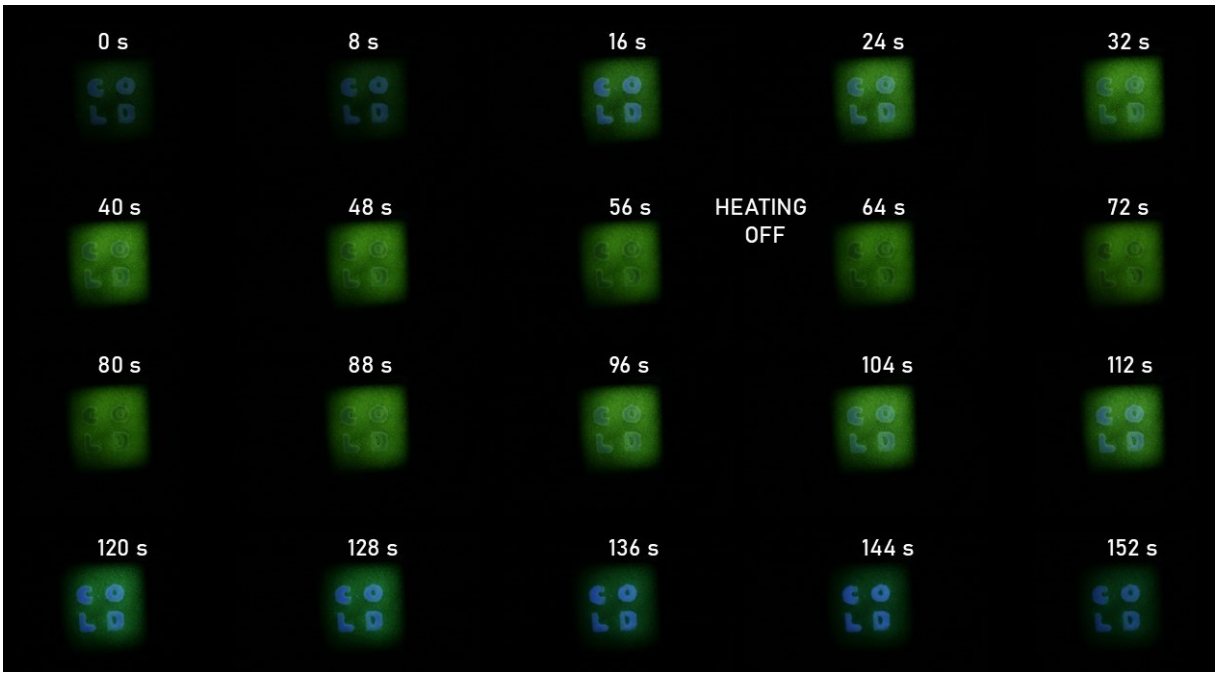

Figure S25. Photos of the luminescence from the pattern obtained as a function of time after turning of the heat gun.

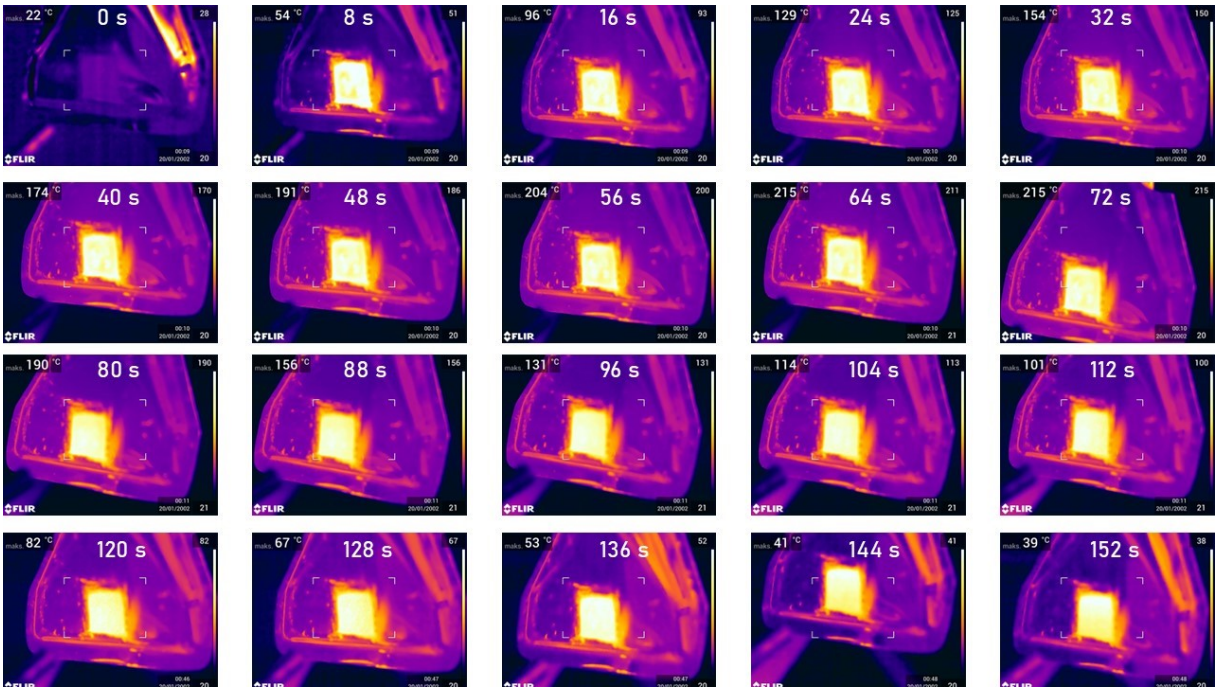

Figure S26. Photos from the thermovision camera of the pattern obtained as a function of time after turning of the heat gun.

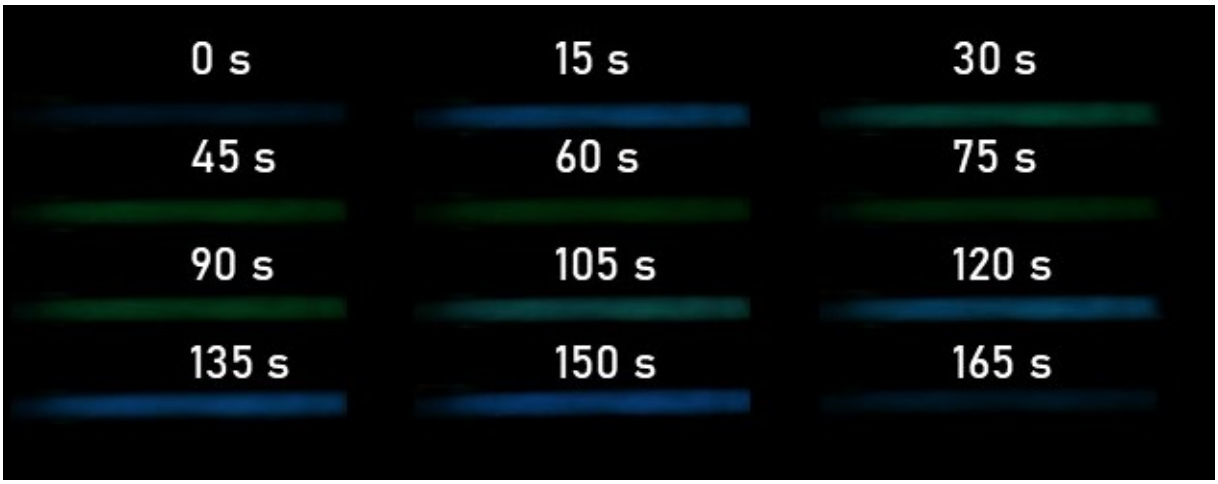

Figure S27. Photos of the luminescence of the strip of $LiYO_2$:0.1%Tb^{3+} phosphor deposited on the metal nozzle of the heat gun captured as a function of time.

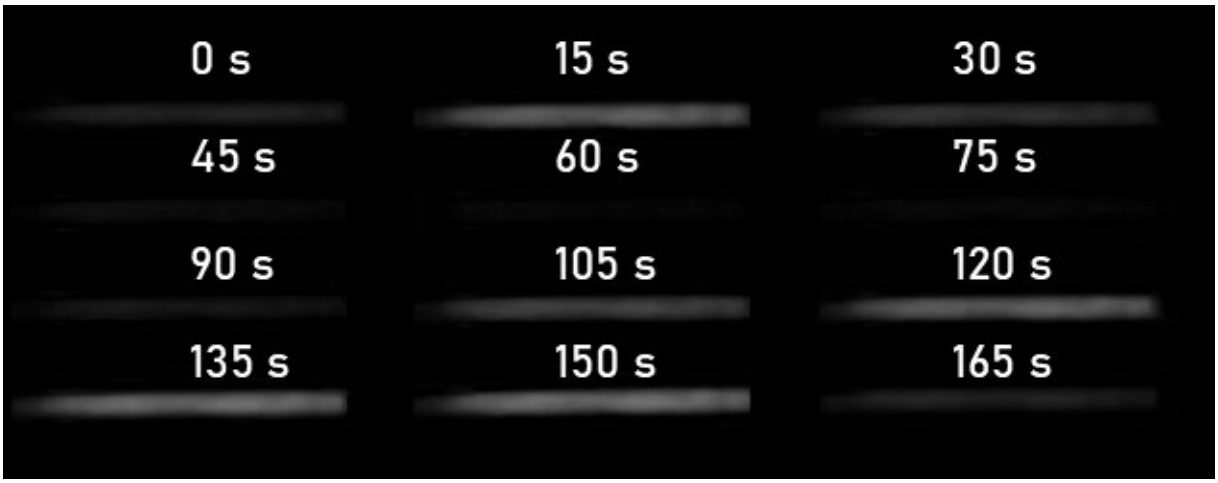

Figure S28. The intensity maps recorded in the B channel obtained from photos of the luminescence of the strip of $LiYO_2$:0.1%Tb^{3+} phosphor deposited on the metal nozzle of the heat gun captured as a function of time.

Figure S29. The intensity maps recorded in the G channel obtained from photos of the luminescence of the strip of $LiYO_2$:0.1%Tb^{3+} phosphor deposited on the metal nozzle of the heat gun captured as a function of time.

Figure S30. The intensity maps recorded in the R channel obtained from photos of the luminescence of the strip of $LiYO_2$:0.1%Tb^{3+} phosphor deposited on the metal nozzle of the heat gun captured as a function of time.

Calibration curve used to convert G/B maps into thermal maps:

$$T = 92.29 + 0.04241 \cdot (G/B) - 2.17 \cdot 10^{-6} \cdot (G/B)^2 + 5.11 \cdot 10^{-11} \cdot (G/B)^3 - 4.25 \cdot 10^{-16} \cdot (G/B)^4 \quad \text{(S1)}$$

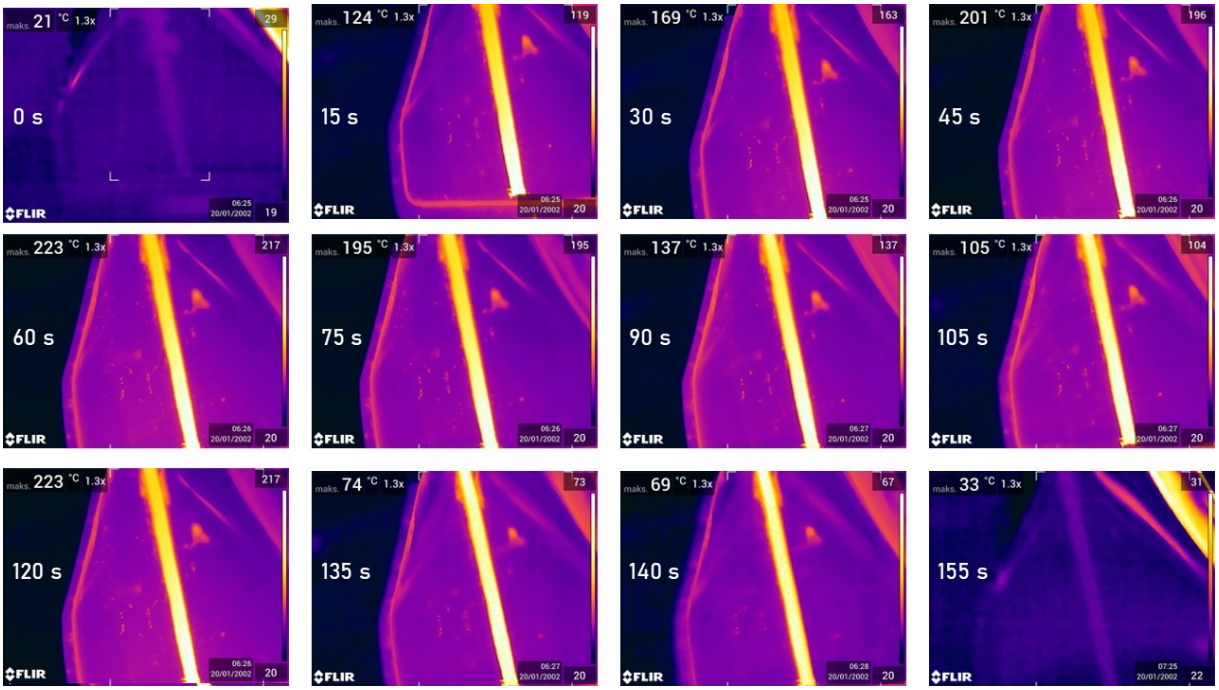

Figure S31. Photos from the thermovision camera of the luminescence of the strip of $LiYO_2$:0.1%Tb^{3+} phosphor deposited on the metal nozzle of the heat gun captured as a function of time.